Original research

In vitro and in silico assessment of flow modulation after deploying the Contour Neurovascular System in intracranial aneurysm models

Jana Korte ,[1,2] Franziska Gaidzik ,[1,2] Naomi Larsen ,[3] Erik Schütz,[2] Timo Damm,[4] Fritz Wodarg ,[3] Jan-Bernd Hövener,[4] Olav Jansen,[3] Gábor Janiga ,[1,2] Philipp Berg ,[2,5] Mariya S Pravdivtseva [4]

ABSTRACT

Background The novel Contour Neurovascular System (Contour) has been reported to be efficient and safe for the treatment of intracranial, wide-necked bifurcation aneurysms. Flow in the aneurysm and posterior cerebral arteries (PCAs) after Contour deployment has not been analyzed in detail yet. However, this information is crucial for predicting aneurysm treatment outcomes.

Methods Time-resolved three-dimensional velocity maps in 14 combinations of patient-based basilar tip aneurysm models with and without Contour devices (sizes between 5 and 14 mm) were analyzed using four-dimensionsal (4D) flow MRI and numerical/image-based flow simulations. A complex virtual processing pipeline was developed to mimic the experimental shape and position of the Contour together with the simulations.

Results On average, the Contour significantly reduced intra-aneurysmal flow velocity by 67% (mean w/ = 0.03m/s; mean w/o = 0.12m/s; p-value=0.002), and the time-averaged wall shear stress by more than 87% (mean w/ = 0.17Pa; mean w/o = 1.35Pa; p-value=0.002), as observed by numerical simulations. Furthermore, a significant reduction in flow (P<0.01) was confirmed by the neck inflow rate, kinetic energy, and inflow concentration index after Contour deployment. Notably, device size has a stronger effect on reducing flow than device positioning. However, positioning affected flow in the PCAs, while being robust in effectively reducing flow.

Conclusions This study showed the high efficacy of the Contour device in reducing flow within aneurysms regardless of the exact position. However, we observed an effect on the flow in PCAs, which needs to be investigated further.

WHAT IS ALREADY KNOWN ON THIS TOPIC

⇒ Flow modulation is an effective treatment for wide-necked aneurysms. The Contour Neurovascular System (Contour) is a novel, half-sphere-shaped, flow-modulating device that is placed in the aneurysm neck and comes in different sizes.

WHAT THIS STUDY ADDS

⇒ Intra-aneurysmal flow modulation and the effect of different device sizes and positions were quantified for the first time.

⇒ Four-dimensional flow MRI and computational fluid dynamics were used to obtain time-resolved, three-dimensional maps of the flow inside patient-derived aneurysm models with and without the Contour device.

⇒ The Contour device induced considerable flow reduction for all sizes and deployments.

HOW THIS STUDY MIGHT AFFECT RESEARCH, PRACTICE OR POLICY

⇒ The flow reduction caused by the Contour device was constant and above 60%, regardless of the exact positioning of the device within a 5° angle, possibly averting the need for repeated device repositioning. However, the Contour positioning influences the flow division into the posterior cerebral arteries (PCAs), which requires further investigation. Moreover, the effect of stronger Contour dispositioning (higher that 5°) on aneurysm and PCA flow is unknown.

INTRODUCTION

Intracranial aneurysms (IAs) carry the risk of rupture and need to be identified and treated if this risk is high.[1–3] Neurovascular hemodynamics play a vital role in IA formation and rupture.[4] Indeed, coil embolization has become an established technique for endovascular treatment of IA.[5] However, embolization of wide-necked bifurcation aneurysms (WNBAs) with coils is more challenging as it requires assisting devices such as stents or balloons and results in relatively low occlusion (40%) and high complication (21%) rates.[6] Intrasaccular flow disruptors such as the Woven EndoBridge (WEB; Microvention/Terumo, Aliso Viejo, CA) were designed as single implants to simplify endovascular WNBA treatment.

Recently, a new intrasaccular device, called Contour Neurovascular System (Contour, Cerus Endovascular, Fremont, CA), was developed. Initial studies showed the efficacy and safety of treating unruptured IAs with this device, including WNBAs.[7–11] Moreover, Contour has been used to treat acutely ruptured aneurysms both as a stand-alone device and in combination with coils.[12–15] A systematic review based on

► Additional supplemental material is published online only. To view, please visit the journal online (http://dx.doi.org/10.1136/jnis-2023-020403).

[1]Laboratory of Fluid Dynamics and Technical Flows, University of Magdeburg, Magdeburg, Germany
[2]Research campus STIMULATE, University of Magdeburg, Magdeburg, Germany
[3]Department of Radiology and Neuroradiology, University Medical Center Schleswig-Holstein (UKSH), Kiel, Germany
[4]Section Biomedical Imaging, Molecular Imaging North Competence Center (MOIN CC), Department of Radiology and Neuroradiology, University Medical Center Schleswig-Holstein (UKSH), Kiel University, Kiel, Germany
[5]Department of Healthcare Telematics and Medical Engineering, University of Magdeburg, Magdeburg, Germany

Correspondence to
Jana Korte; korte.j@outlook.com

JK and FG contributed equally. PB and MSP contributed equally.

Received 6 April 2023
Accepted 15 July 2023
Published Online First 18 October 2023

To cite: Korte J, Gaidzik F, Larsen N, *et al*. *J NeuroIntervent Surg* 2024;**16**:815–823.

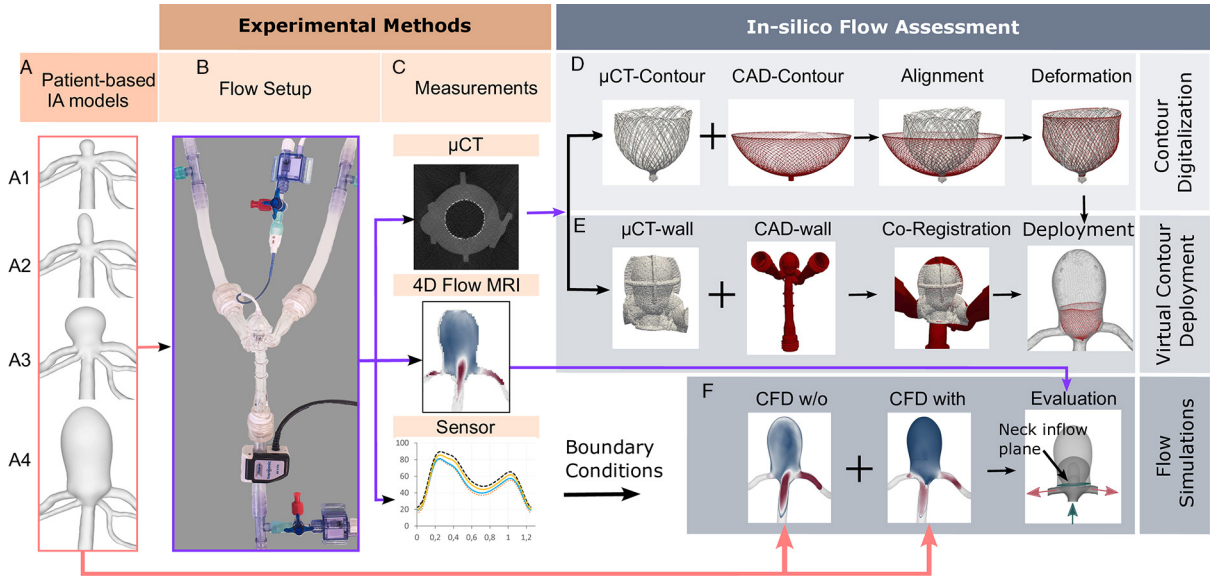

Figure 1 Processing pipeline used to mimic the experiments by numerical CFD simulations. On the experimental side, patient-based IA models (A) and the corresponding flow setup (B) were used to acquire μCT and 4D flow MRI data (C). Flow and pressure sensors provided the boundary conditions for CFD. For placing the Contour in the virtual aneurysm model, first, the CAD-model of the Contour was deformed according to μCT images (D). Next, the position of the Contour inside the model was determined from μCT data and the deformed Contour accordingly placed (E). Finally, CFD simulations were carried out and compared with 4D flow MRI findings (F). CAD, Computer Aided Design; CFD, computational fluid dynamic; 4D, four-dimensional; IA, intracranial aneurysm; μCT, micro-CT; w/o, without.

six studies,[7–9 11 14 15] including 131 IAs treated with either Contour or Contour and coils, showed a pooled adequate occlusion rate of 84%.[16]

Experience with the Contour device is limited. Most of the aforementioned studies had a retrospective design, including angiographic (X-ray-based) and clinical neurological follow-up. Only one study discussed MRI follow-ups, reporting strong metal artifacts originating from the implant.[8]

The primary purpose of the Contour is to disrupt and divert the flow from an IA. However, to the best of the authors' knowledge, the direct flow changes caused by the Contour have not been evaluated yet. In a previous experimental study, the washout time of an angiographic contrast agent observed with digital subtraction angiography (DSA) was used as a surrogate marker for the effectiveness of the device.[17] However, the analysis was limited to a two-dimensional (2D) evaluation of the flow and might be operator dependent.

Therefore, this study aimed to quantify the intra-aneurysmal changes in flow, induced by placing the Contour in IA models, which were based on patient data, using time-dependent, high-dimensional computational fluid dynamic (CFD) simulations. Furthermore, four-dimensional (4D) flow MRI experiments were conducted to assess the feasibility of evaluating IA hemodynamics with in vivo modality in the presence of the Contour device.

MATERIALS AND METHODS

In this study, a complex processing pipeline was developed, starting with four patient-based basilar tip aneurysm models. The processing pipeline, comprising the experimental method and the in-silico flow assessment, is shown in figure 1. Details will be explained within the following subsections.

Patient-based aneurysm models

The four patient-based basilar tip aneurysm models A1–4 (figure 1A), were designed and three-dimensionally (3D) printed in-house[17 18] (for details see online supplemental file S1 and table S1). The diameters (height, neck, dome) of the IA sac were 3.5×2.7×3.2 mm (A1), 6.9×2.8×3.3 mm (A2), 8.4×6.7×8.4 mm (A3), and 16.4×9.2×10.2 mm (A4), respectively (figure 1A). IA models were designed as WNBAs with a comparable dome-to-neck ratio (1.2±0.1). All models shared the same parent vessel and posterior cerebral arteries. The models ready for 3D printing are freely available at Zenodo.[19]

The virtual model used for CFD simulations is slightly different from the one used for 4D flow MRI measurements. Namely, superior cerebral arteries (SCA) were initially modelled for experiments, but due to their small size they were partially occluded during the 3D printing process. Thus, to preserve the comparability between 4D flow MRI and CFD the SCAs were removed from the virtual models used for CFD analysis. The exclusion of the branches does not affect the change of the hemodynamics in the IAs by placement of the Contour system analyzed in this study (see online supplemental table S2, online supplemental figure S1).

Experimental methods

Flow setup and in vitro device deployment

IA models were integrated into a closed cycle flow setup and supplied with saline solution at a mean flow rate of 150 mL/min to mimic flow in the basilar artery observed in vivo (Ismatec MCP Standard, Cole Parmer, IL).[20] Time-dependent flow and pressure waveforms were measured at the inlet and outlets (see online supplemental figures S2/S3) and only pressure at the tip of the IA sac using flow and pressure sensors (ME8PXL-M12, Transonic System Inc, NY; PRESS-N-000; PendoTech, NJ), respectively (figure 2B).

Ten Contours (C1–10) of three sizes—5 mm (C1–5), 11 mm (C6–9), and 14 mm (C10)—were deployed into IAs (A1–4) under fluoroscopy (Allura Xper FD, Philips, The Netherlands) by an experienced neuroradiologist (>10 years of experience, FW) (deployment: A1: C1–2; A2: C3–5; A3: C6–9; A4: C10; for details see online supplemental file S2).

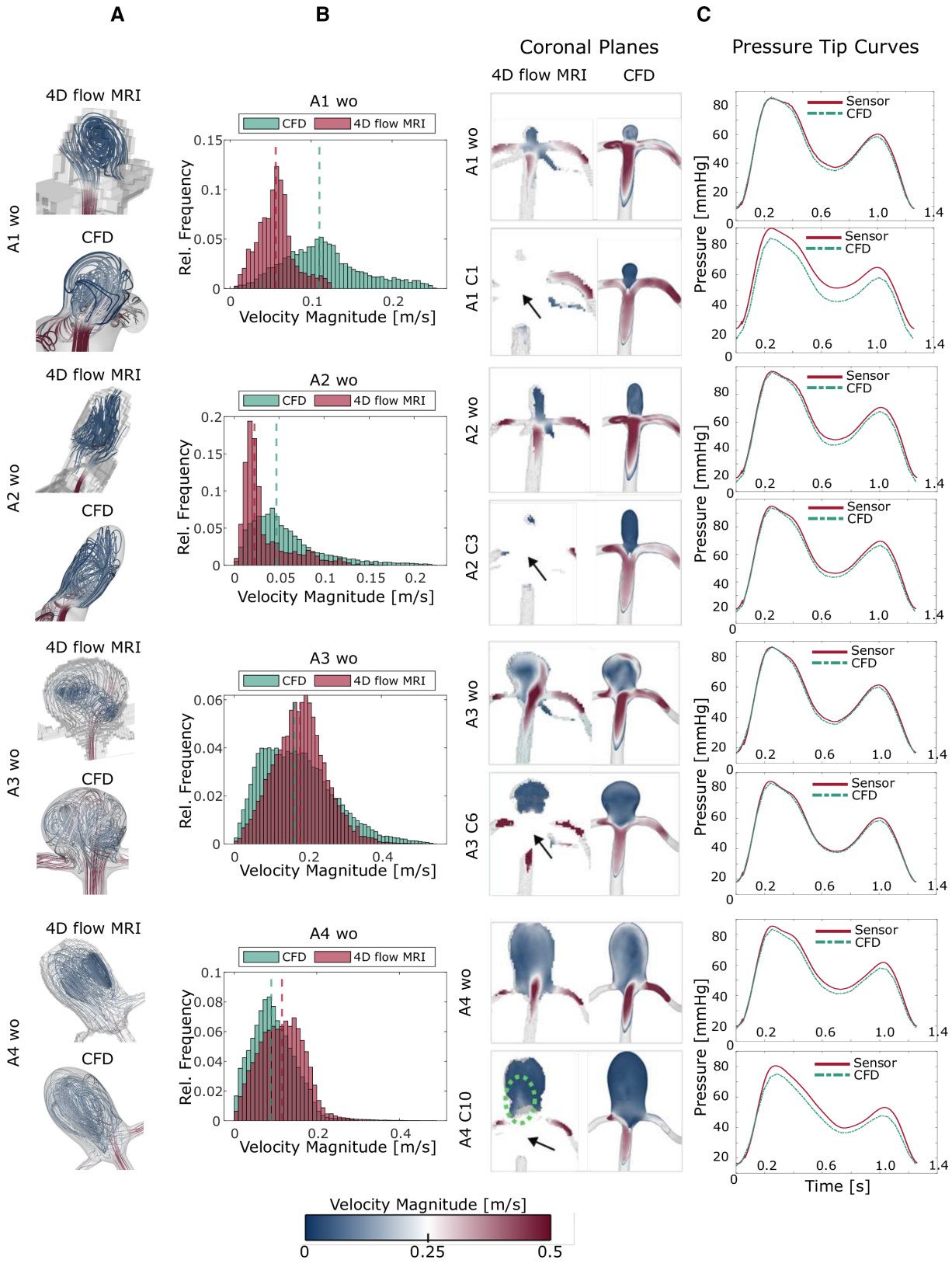

Figure 2 Qualitative and quantitative comparison of 4D flow MRI and CFD velocity fields. For each aneurysm size, one representative case is shown. (A) Velocity streamlines before Contour deployment for A1–A4. (B) Histogram plots before Contour deployment of the 4D flow MRI and CFD velocity values after interpolating them on the same grid. Median values are displayed with a dashed vertical line. (C) The velocity magnitude in the coronal plane is displayed on the left (top row: without Contour, bottom row: with Contour) for both modalities. Results without Contour show high correspondence between 4D flow MRI and CFD. Metal artifacts caused signal voids in the model with Contour and partly no velocities could be obtained in 4D flow MRI for these cases (black arrows), despite for IA sac of A4 C10 (green dashed circle). The highly-resolved CFD data can provide a detailed view of the flow in the aneurysm with Contour. Pressure values at the aneurysm tip (sensor data and CFD) are displayed on the right. CFD, computational fluid dynamic; 4D, four-dimensional.

4D flow MRI

4D flow MRI data were acquired by using a 3T whole-body MR system equipped with a 32-channel head coil (Ingenia CX, R5 V6.1, Philips Healthcare, Best, The Netherlands). Velocities were quantified with a time-resolved phase-contrast MR sequence with 3D coverage (4D flow MRI, figure 1C). Temporal and spatial resolution was 63 ms and $(0.75\ mm)^3$, respectively. The velocity-encoding parameter was set to 75 cm/s for all IA models, about 10% higher than the maximum velocity observed at the inlet vessel without Contour. Linear offset phase correction, velocity aliasing, and vessel masking were performed using GTflow (V3.1.12, Gyrotools, Switzerland) (for details see online supplemental file S3).

In silico flow assessment

To accurately mimic the exact shape and position of the Contour by using CFD, the Contour was digitalized and virtually deployed (figure 1) as described in detail below.

Contour digitalization

To develop a digital Contour ready-to-be-placed in the IA model (figure 1D), first, micro-CT (μCT) was acquired from all Contours inside the IA models (a vivaCT 80; Scanco Medical AG, Brüttisellen, Switzerland; 45 keV, 80 mm field of view, reconstructed to 26 µm isotropic voxel size). Here, a scalar mask based on signal intensity was created using a threshold-based, seeded, region-growing algorithm.[21] Next, the mesh was generated based on the scalar mask using a marching cubes algorithm.[22]

Second, a 3D computer-aided Contour design (CAD-Contour) was created based on 2D representations of the unconstrained device provided by the manufacturer (Fusion 360 2.0, Autodesk Inc, USA). Specifically, the CAD-Contour consisted of 72 circles equally spaced from each other connected at the base of the device, adjacent to the radiopaque marker. In this way, an unconstrained model of the Contour was obtained, which changed after deployment (see figure 1D).

Thus, and third, to accurately obtain the shape of the μCT-Contour, the CAD-Contour was non-rigidly transformed to the μCT data, by alignment of the radiopaque markers. Then, the CAD-Contour was adapted to the shape of the μCT-Contour using a lattice modifier (Blender, Blender Foundation, v3.1., Amsterdam, The Netherlands). The modifier smoothly deformed the CAD-Contour according to the shape of the μCT-Contour. Hence, a constrained configuration of the CAD-Contour was achieved, which was used for the highly resolved CFD simulations.

The direct use of Contour segmented from µCT images was not feasible due to the limited spatial resolution of the μCT which resulted in segmentation artefacts such as substantially increased wire thickness of the Contour and the presence of fully occluded Contour segments (see online supplemental file S4, online supplemental table S3, online supplemental figure S4).

Virtual device deployment

The virtual IA models and the constrained CAD-Contours were located in different coordinate systems. To ensure that the CAD-Contours were correctly positioned within the IA sac, first, the 3D-printed wall of the aneurysm model was segmented from the same μCT images as the μCT-Contour (figure 1E). The μCT-wall was aligned with the CAD-wall using an iterative, closest-point algorithm (MeshLab 2022.02, ISTI - CNR, Pisa, Italy). Second, the resulting transformation matrix was applied to the CAD-Contour. As CAD-wall and CAD-aneurysm lie in an identical coordinate system, this single transformation ensured that the Contour was correctly placed within the CAD-aneurysm.

CFD simulations

Numerical CFD simulations were carried out using a finite volume solver (StarCCM+2021.3 v16.6, Siemens, Erlangen, Germany). Boundary conditions obtained in the experiments (figure 1C) were applied at the extruded inlet and outlets (measured massflow and pressure waveforms) of the IA models. Furthermore, rigid vessel walls and the mimicking fluid properties were used (water: density = 998 kg/m^3, dynamic viscosity = 0.001 Pa·s).

Spatial discretization of the IA and CAD-Contour models was performed with a base cell size of 0.1 mm at the aneurysm sac and parent vessel, while 0.02 mm was chosen at the Contour struts and 0.3 mm at the vessel extrusions. The total cell count within the IA models with Contour ranged from 8.8 million (A1) to 11.6 million cells (A4). The models without Contour featured a total cell count of 2.4 to 4 million cells.

In total, 14 time-dependent CFD simulations were carried out (four without: A1–4; 10 with Contour: A1 C1–2, A2 C3–5, A3 C6–9, A4 C10). Temporal resolution was 1 ms over three cardiac cycles, whereas only the last cycle was analyzed. Cycle length of 1.26 s was determined from the experiment.

Data analysis

The experimental 4D flow MRI results were compared with the calculated CFD velocity by interpolating the velocity fields from 4D flow MRI and CFD inside the untreated IA sac onto a grid with the base size of 0.3 mm. Next, the changes in the intra-aneurysmal flow after placing the Contour were evaluated. Namely, oscillatory shear index (OSI), oscillatory velocity index (OVI), neck inflow rate (NIR), time-averaged wall shear stress (TAWSS), velocity (V), kinetic energy (KE), inflow concentration index (ICI), and aneurysm turnover time (TOT), which is the aneurysm sac volume divided by the NIR, were evaluated (see online supplemental file S5). For each parameter (P) with (w/) and without (w/o) Contour, the treatment effect (TE) was calculated for C1–10, respectively.

$$TE_p = \frac{Mean\ P_{w/} - Mean\ P_{w/o}}{Mean\ P_{w/o}} \quad (1)$$

The outlet flow of left and right posterior cerebral arteries (PCAs) was normalized by the total outflow. Statistical analysis was performed in MATLAB (MATLAB R2022a, The MathWorks, Natick, MA), using the paired Wilcoxon test. With the Bonferroni correction the P value was set to 0.007. The chosen inflow plane for calculating NIR is shown in figure 1F.

RESULTS

Flow comparison between 4D flow MRI and CFD

Without Contour

The velocity fields calculated in the IA geometries without Contour were similar to those measured with 4D flow MRI (figure 2A, streamline and velocity magnitude images). For A4, the flow jet entering the aneurysm sac was observed in both modalities. In CFD, the jet appears to be broader and slightly shifted to the right side of the IA's wall. In A3, the simulated flow jet was clearly visible and the 4D flow MRI did not distinctly show the flow attached to the wall. However, the overall flow field remained similar between 4D flow MRI and CFD. For the smaller models (A1 and A2), the highly resolved CFD simulations showed fine velocity structures, which were not visible on the 4D flow MRI velocity maps. Generally, 4D flow MRI results suffered from limited spatial resolution, especially for

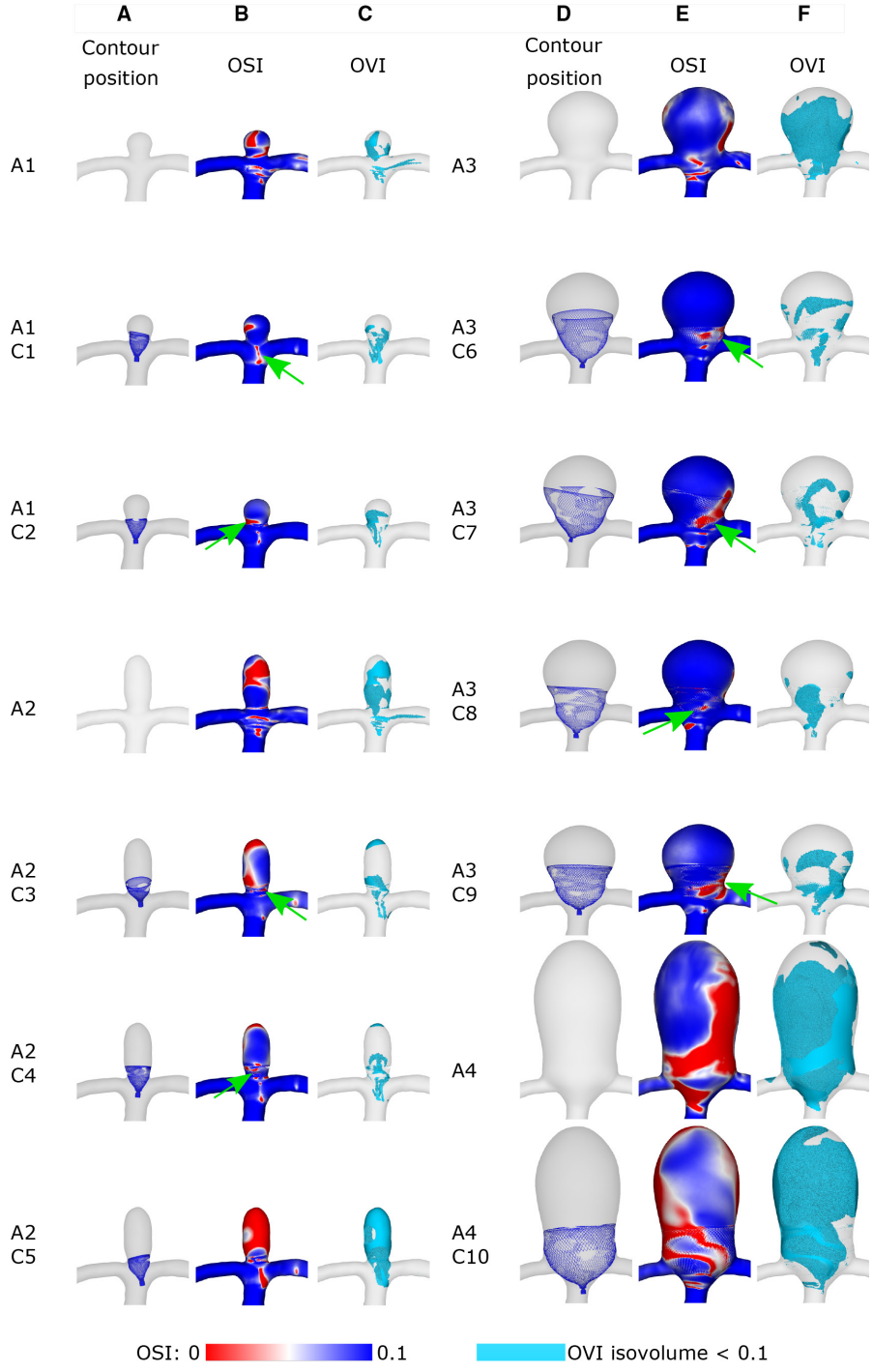

Figure 3 Virtual vascular model with and without Contour (A, D), oscillatory shear index (B, E, OSI), and oscillatory velocity index (C, F, OVI). Note the variation in position and orientation of the device. Green arrows highlight the higher OSI in the regions close to the Contour locations.

small aneurysms (A1 and A2), and a velocity noise that is comparable to the velocities observed at the center of the aneurysm and along the walls. Quantitatively, as shown in the histogram plots in figure 2B, two smaller sized IAs (A1 and A2) had a higher relative frequency for low velocity values measured with 4D flow MRI (median 0.056 m/s for A1 and 0.023 m/s for A2) when compared with CFD (median 0.11 m/s for A1 and 0.047 m/s for A2). For A3 the median values for both modalities were similar (median 0.179 m/s for 4D flow MRI and 0.163 m/s for CFD), whereas for A4, the measured values were slightly higher (median 0.115 m/s for 4D flow MRI and 0.09 m/s for CFD).

With Contour

Strong MRI artifacts originating from the radiopaque marker of the Contour (figure 2C, black arrows) were observed on 4D flow MRI images. All 4D flow MRI data obtained in the vicinity of strong artifacts must be analyzed carefully, as the artifacts affect the phase-based flow encoding. Furthermore, the strong flow reduction inside the IA leads to near-zero velocities in the IA sac, which are close to the 4D flow MRI velocity noise limit. All of this prevents the use of 4D flow MRI to assess post-treatment IA hemodynamics, especially for small IAs. As a result, the analysis of velocity fields measured with MRI close to the Contour is impossible and limited only to the artifact-free area.

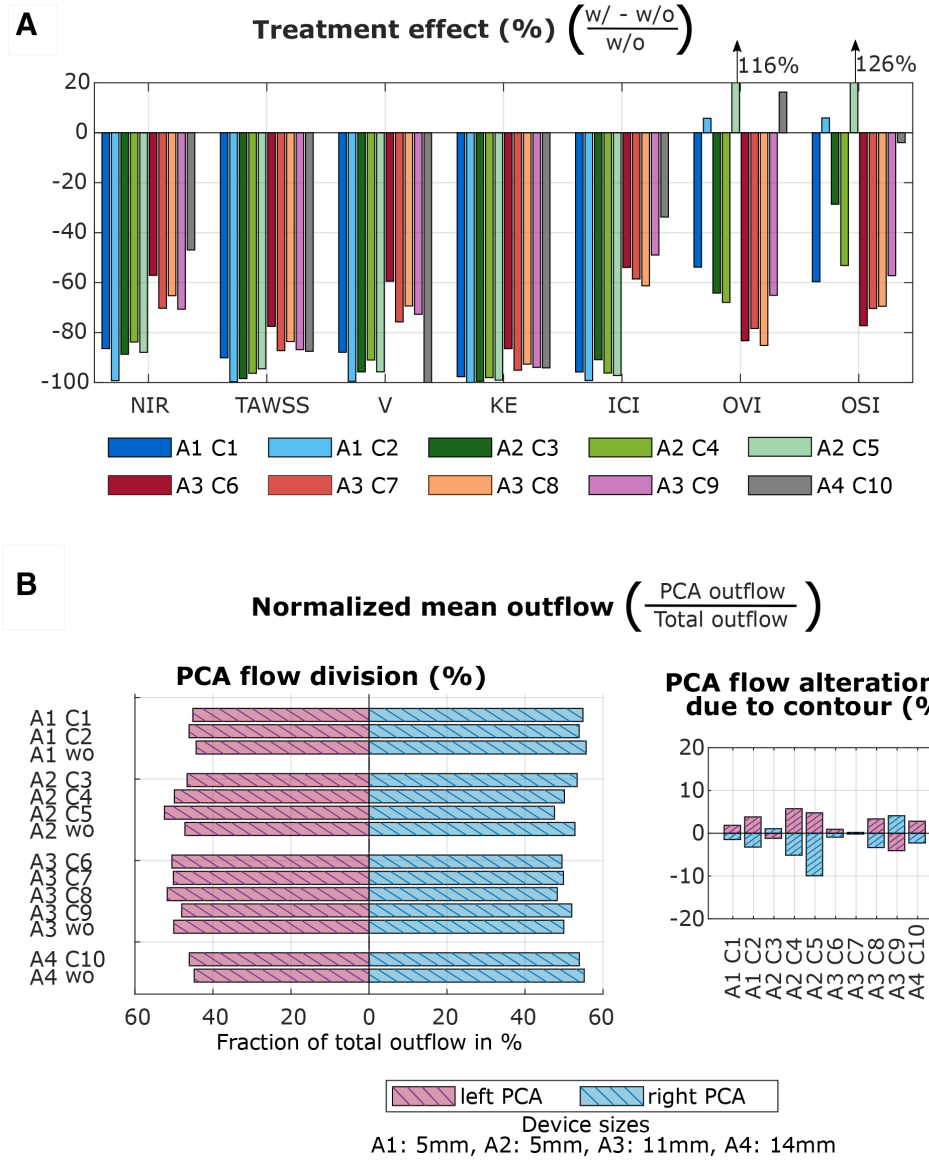

Figure 4 Quantification of flow reduction of the Contour. (A) Treatment effect for chosen hemodynamic parameters in %. (B) Normalized mean outlet flow division with flow data derived from sensor measurements in % and the treatment effect onto the outlet flow division for the left and right PCAs. ICI, inflow concentration index; IR, neck inflow rate (mL/s); KE, kinetic energy (Pa); OSI, oscillatory shear index; OVI, oscillatory velocity index; PCA, posterior cerebral artery; TAWSS, time-averaged wall shear stress (Pa); V, velocity (m/s); w/, with Contour; w/o, without Contour.

For case A4 C10, flow division on the left and right PCAs revealed higher flow through the left PCA with both modalities (figure 2C, coronal plane, green circle). This is offering the perspective that measuring flow by 4D flow MRI close to the implant is not completely impossible. Overall, the strong flow reduction induced by the Contour was detected by CFD and 4D flow MRI.

Remarkably, the pressure curves acquired from CFD and sensor measurements showed excellent agreement throughout the whole cardiac cycle for all cases (mean deviation of 6% without and 8% with Contour).

Intra-aneurysmal device efficacy

The majority of the devices were located centrally in the parent vessel (figure 3A/D). A2 C5 and A4 C10 were slightly shifted towards the right and A3 C7 to the left PCA bifurcation. Compared with a vertical middle line through the aneurysm model, the implanted devices were shifted by an angle between 1° and 5°. Concerning the flow parameters OSI (figure 3B and E) and OVI (figure 3C and F), the intra-aneurysmal reduction after deployment was visible for C1–4 and for C6–9. Concerning C5 and C10, OSI and OVI were increased, respectively. For all cases with Contours, except C5 and C10, OSI and OVI were higher, especially around the location of the Contour (see green arrows), and lower within the aneurysm dome compared with those without Contour.

Effect of device size

A greater reduction in NIR, TAWSS, V, KE, and ICI was found after deploying a smaller-sized (83–99%, device size 5 mm, A1/A2 C1–5) than a larger-sized Contour (48–95%, device size 11 mm, A3 C6–9), as represented in figure 4A. For A3 (C6–9) a high reduction of 86–95% is visible only for KE, and for C10 one of 87–100% for TAWSS, V, and KE. Still, an overall reduction of more than 40% is visible for C1–10 for these parameters, except for ICI within C10. The reduction in OSI and OVI was stable at more than 58% for A3 (C6–9). In contrast, this

Table 1 Comparison of hemodynamic mean results between with (w/) and without (w/o) Contour including SD and P value

	Mean w/	±SD w/	Mean w/o	±SD w/	P value
NIR* (mL/s)	0.53	±0.62	1.46	±1.28	0.002
TAWSS* (Pa)	0.17	±0.17	1.35	±0.73	0.002
V* (m/s)	0.03	±0.03	0.12	±0.05	0.002
KE* (J)	1.06	±1.29	16.03	±11.9	0.002
ICI*	0.64	±0.84	1.43	±1.23	0.002
OVI	0.04	±0.04	0.06	±0.01	0.16
OSI	0.05	±0.04	0.08	±0.02	0.105
TOT* (s)	3.46	±3.9	0.28	±0.15	0.002

Significant differences are marked with an asterisk*.
ICI, inflow concentration index; KE, kinetic energy; NIR, neck inflow rate; OSI, oscillatory shear index; OVI, oscillatory velocity index; TAWSS, time-averaged wall shear stress; TOT, aneurysm turnover time ; V, velocity.

reduction was lower in A1/A2/A4 than in all cases of A3 except C9 or OVI/OSI even increased.

Effect of the aneurysm height

The height of the aneurysm sac A2 was almost two times larger than A1 (6.9 mm vs 3.5 mm), while the size of the neck and dome was comparable. Therefore, the same Contour size was implanted. Remarkably, no specific difference in the treatment effect attributed to the different aneurysm heights was found.

Effect of the device positioning

Four devices (C6–9) were placed in A3. Here, flow reduction ranged within a difference of Δ 8.63% (KE) and Δ 13.53% (NIR) to Δ 20.06% (OVI). Detailed TE values can be found in online supplemental table S4.

Significance

Mean NIR, TAWSS, V, KE, ICI, and TOT were significantly higher ($P<0.01$) for cases without Contour, while OVI ($P=0.16$) and OSI ($P=0.11$) did not differ significantly between groups (see table 1 and online supplemental figure S5).

Flow changes in the posterior cerebral arteries

The left outflow varied between 44% and 52% and the right between 47% and 56% (figure 4B). The TE on the outflow was low at 0.1–5.7%; only in C5 was the effect stronger (TE=10%). C5 was also most shifted to the left PCA (see figure 3). C6/C7 as compared with C8/C9 had a smaller effect on the flow alteration and the Contour was placed higher inside the aneurysm so that the PCAs were less affected.

DISCUSSION

Endovascular treatment of WNBAs with Contour is a novel technique that has not been studied well yet, but the treatment results in high IA occlusion rates and safety.[11 14 16] In this study, the intra-aneurysmal flow reduction as well as flow alterations in the PCAs, that were affected by the Contour, were analyzed. Aneurysm models representing different shapes and sizes, together with the effect of different Contour deployments in the same geometry, were investigated. In contrast to existing minimally invasive techniques, Contour can treat IAs with complex shapes regardless of aneurysm height and does not require post-interventional antiplatelet therapy.[7 8]

Comparison of 4D flow MRI and CFD

Due to strong metal artifacts within 4D flow MRI data caused by Contour, it is advantageous to use CFD for analyzing the effect of Contour deployment (figures 2 and 3). Being the first-ever numerical study analyzing flow alterations by Contour, it was necessary to compare the CFD results qualitatively with measured 4D flow MRI velocity fields in the metal artifacts-free regions and quantitatively with measured pressure sensor data and 4D flow MRI data before Contour deployment (figure 2). Velocity-encoded streamlines and histogram plots showed the highest differences between both modalities in the smaller IAs (A1 and A2). This is attributed to the relatively higher influence of measurement noise, 3D-printing inhomogeneities or registration errors that influence the acquired values. Furthermore, the SCAs, which were partly present in the 3D printed models but removed from the virtual CFD model, might cause a deviation. However, for the larger IA models (A3 and A4) the velocity fields are more similar and the main characteristics (flow jet or median values) are nearly in accordance. The findings are in agreement with Sindeev *et al*, who showed the compatibility of MRI and CFD within IAs.[23]

Intra-aneurysmal flow

The subsequent in-depth analysis revealed a strong flow reduction in all cases for NIR, ICI, and TAWSS and the intra-aneurysmal flow (KE and V). According to Ouared *et al*,[24] for flow diverter stent (FDS) deployment, a reduction in velocity greater than 35% can be considered as a successful occlusion of an aneurysm. In the present study, velocity reduction was higher than 60% for all cases and thus indicates a potentially effective occlusion, confirming the findings of recent in vivo studies.[11 14 16]

Aneurysm occlusion is also ensured by the use of a WEB.[25 26] However, the sizing of the device depends on the aneurysm width and height, where height is usually limited to 10 mm. The Contour is characterized by its height-independent implementation as it is placed directly at the neck,[15] and aneurysm height did not affect the efficacy of the Contour.

Comparing the TE between Contour and FDS, the latter shows a lower reduction in NIR (ΔNIR >29%), TAWSS (ΔTAWSS >23%), and V (ΔV >20%) within the aneurysm.[27] Kulcsár *et al* reported that TAWSS and V reduction cause IA occlusion, but they could not determine a predictive threshold value.[28] FDS deployment carries the risk of occluding small lateral branches and FDS are difficult to use in bifurcation aneurysms,[29] which does not apply to the Contour.[11] Nevertheless, the Countour is not well suited for small-neck aneurysms in contrast to in-vessel devices such as FDS.[8]

Compared with intrasaccular coiling, the Contour showed a similarly effective flow reduction. Still, this reduction after coiling is not significantly related to aneurysm occlusion.[30] Coiling carries the advantage of conserving parent vessel flow, but implementation is more complex and not suitable for WNBAs without the use of additional stents or balloons.[10]

In contrast to the NIR, TAWSS, and V reductions, Contour deployment enriches the oscillatory effects inside the aneurysm in some cases (figure 4A and table 1). This finding is in line with a previous study in which OVI increased inside the IA after implanting an FDS.[31] Roloff *et al*[31] found that FDS malpositioning increases OSI, but has no major effect on flow reduction. This leads to the assumption that adequate positioning of the Contour could ensure a decrease in OSI/OVI (figures 3 and 4, table 1). Moreover, high OSI correlated with recanalization after coil embolization.[32]

The calculated aneurysm TOT (table 1) is a measure of flow stasis and has been studied as a potential marker for thrombus formation, and subsequently IA occlusion.[33–36] The mean TOT in all models were significantly higher after Contour deployment, thus confirming the positive treatment effect of the Contour and increasing the chance of thrombus formation. These results are in accordance with the washout time calculations observed with DSA in the same aneurysm models.[17]

Outlet flow alteration

Furthermore, due to its shape, according to our findings, the Contour disturbs outlet vessel flow by altering flow division into the PCAs, depending on the positioning (figure 4B). Still, the intra-aneurysmal flow reduction remained independent from the device positioning. Thus, an angular shift of 5° affects flow alteration through the PCAs but not intra-aneurysmal flow reduction. However, it remains uncertain if this result can be replicated in vivo. Likely, the deployment of the Contour would not alter the flow demand in the distal vascular beds, resulting in similar outflow boundary conditions. As a result, minimal changes in flow division among the PCAs can be expected following Contour deployment. Therefore, these findings require further investigation. In comparison, parent vessel flow is conserved by deploying WEB and coiling as no part of the device is placed outside the IA.[25 37]

Limitations

This study has several limitations. First, 4D flow MRI might be affected by insufficient spatial resolution,[38] especially within small IAs. Moreover, MR images were impaired by metal artifacts, mostly due to the radiopaque marker. The metal artifacts caused by Contour seem to be drastically stronger than for FDS.[39] Thus, comparison of the CFD simulations to 4D flow was mainly limited to the cases without Contour and to the pressure sensor measurements.

Second, while efforts were made to realistically mimic the Contour placement, minor misalignments were observed. Still, it was the best approach available since direct use of µCT segmented Contours was not possible due to segmentation artifacts (online supplemental file S4). Nevertheless, this is the first study to virtually mimic Contour placement realistically, enabling numerical analysis of relevant hemodynamic parameters.

Third, the input flow waveforms for CFD were not patient-specific but mimicked the shape of a cardiac cycle and mean flow rate reported in a basilar artery in vivo (see online supplemental figures S2 and S3).

Fourth, to compare hemodynamic parameters between the current numerical study and a previous experimental study[17] (specifically TOT vs washout time (WOT)), a saline solution was utilized for both experiments and CFD simulations. The viscosity of saline differs from that of blood, potentially hindering a direct comparison of the results in this study to in vivo IA hemodynamics. However, additional simulations did not reveal a substantial impact of viscosity on the treatment effect of the Contour analyzed in this study (online supplemental figure S6).

Fifth, only IAs of the basilar artery were considered in this study, and all models had identical parent vessel and posterior cerebral arteries. This limits the generalizability of the obtained results. In addition, SCAs were removed from the virtual IA model due to small vessel diameters and vessel occlusion after 3D printing. This prevented the analysis of flow through SCAs. Nevertheless, the exclusion of the branches did not affect the treatment effect of the Contour in the IA (see online supplemental table S2, online supplemental figure S1).

Sixth, due to the complex workflow and resource-intensive nature of the study, only 10 cases were initially considered. To enhance the robustness of the findings, a larger sample size should be included in future investigations.

Last, this study raises important clinical questions that cannot be fully addressed within the scope of a single study. These include the impact of Contour placement on flow in the PCA, the robustness of the Contour efficiency from device positioning, namely the effect of more pronounced (>5°) device angulation, and the prediction of IA occlusion status based on the flow reduction. Addressing these questions will be the focus of future research.

CONCLUSIONS

In this study, the effectiveness of Contour was shown and, for the first time, flow was analyzed in detail, quantitatively addressing IA flow reduction. Contour reduced intra-aneurysmal velocity and TAWSS for all cases. Overall comparison between with and without Contour showed a significant reduction in the chosen hemodynamic parameters. Device size has a greater effect on reducing flow than does positioning. However, positioning influences the flow division into the PCAs, which requires further investigation.

Correction notice Since this paper first published, the symbol * has been added to the category TOT in table 1.

X Naomi Larsen @naomilarsen6 and Mariya S Pravdivtseva @MPravdivtseva

Acknowledgements We acknowledge Philips Healthcare for support in 4D flow MRI experiments. We thank Cerus Endovascular for providing the Contour Neurovascular System for in vitro testing. We acknowledge support by Kiel University and the Medical Faculty for supporting the Molecular Imaging North Competence Center (MOIN CC) as core facility for imaging in vivo.

Contributors Conceptualization and design: JK, FG, MSP, NL, PB. Implantation of the Contours and choice of the aneurysm models: MSP and FW. Acquisition of MRI data and construction of the 3D printed models: MSP. Acquisition of mCT data: TD. Development of the virtual pre-processing pipeline: JK, FG, ES. Conduction of CFD simulations: JK, FG. Data analysis and interpretation: NL, JK, FG, MP, PB. Data visualization: JK, FG. Statistical analysis: JK. Supervision and funding acquisition: PB, NL, FW, JBH, OJ. Writing – original draft preparation: JK, FG, MSP. Writing – review and editing: JK, FG, MSP, NL, TD, FW, JSH, OJ, PB, GJ. Guarantor: JK. All authors have read and agreed to the published version of the manuscript. JK and FG contributed equally to this paper and share first authorship. MP and PB contributed equally to this paper and share last authorship.

Funding This work was supported by the German Research Foundation (GRK2154: P2b, SPP2311: project no. 465189657), the German Federal Ministry of Education and Research within the Research Campus STIMULATE (grant no. 13GW0473A), and the Bruhn Foundation. MOIN CC was founded by a grant from the European Regional Development Fund (ERDF) and the Zukunftsprogramm Wirtschaft of Schleswig-Holstein (project no. 122-09-053).

Competing interests The author(s) declared the following potential conflicts of interest with respect to the research, of this article: MSP has received a research grant from Cerus endovascular; FW has received fees for consulting and speaking from Balt International SAS and Cerus Endovascular.

Patient consent for publication Not applicable.

Ethics approval Not applicable.

Provenance and peer review Not commissioned; externally peer reviewed.

Data availability statement MRI, CFD, flow and pressure sensor data are available upon reasonable request. Digital aneurysm models ready for 3D printing are available for download at the Zenodo research repository [doi: 10.5281/zenodo.4723100].

ORCID iDs
Jana Korte http://orcid.org/0000-0002-0434-712X
Franziska Gaidzik http://orcid.org/0000-0003-1924-821X
Naomi Larsen http://orcid.org/0000-0002-8782-8278
Fritz Wodarg http://orcid.org/0000-0003-1413-2699
Gábor Janiga http://orcid.org/0000-0002-4560-9640
Philipp Berg http://orcid.org/0000-0003-4140-6771
Mariya S Pravdivtseva http://orcid.org/0000-0001-9442-088X

REFERENCES

1 Wiebers DO, Whisnant JP, Huston J, *et al*. Unruptured intracranial aneurysms: natural history, clinical outcome, and risks of surgical and endovascular treatment. *Lancet* 2003;362:103–10.
2 Hackenberg KAM, Hänggi D, Etminan N. Unruptured intracranial aneurysms. *Stroke* 2018;49:2268–75.
3 Brisman JL, Song JK, Newell DW. Cerebral aneurysms. *N Engl J Med* 2006;355:928–39.
4 Soldozy S, Norat P, Elsarrag M, *et al*. The biophysical role of hemodynamics in the pathogenesis of cerebral aneurysm formation and rupture. *Neurosurg Focus* 2019;47:2019.4.FOCUS19232.
5 Molyneux AJ, Birks J, Clarke A, *et al*. The durability of endovascular coiling versus neurosurgical clipping of ruptured cerebral aneurysms: 18 year follow-up of the UK cohort of the International Subarachnoid Aneurysm Trial (ISAT). *Lancet* 2015;385:691–7.
6 Fiorella D, Arthur AS, Chiacchierini R, *et al*. How safe and effective are existing treatments for wide-necked bifurcation aneurysms? Literature-based objective performance criteria for safety and effectiveness. *J Neurointerv Surg* 2017;9:1197–201.
7 Liebig T, Killer-Oberpfalzer M, Gal G, *et al*. The safety and effectiveness of the Contour Neurovascular System (Contour) for the treatment of bifurcation aneurysms: the CERUS study. *Neurosurgery* 2022;90:270–7.
8 Akhunbay-Fudge CY, Deniz K, Tyagi AK, *et al*. Endovascular treatment of wide-necked intracranial aneurysms using the novel Contour Neurovascular System: a single-center safety and feasibility study. *J Neurointerv Surg* 2020;12:987–92.
9 Bhogal P, Chudyk J, Bleise C, *et al*. Treatment of unruptured, tandem aneurysms of the ICA with a single flow diverter. *Clin Neuroradiol* 2019;29:725–31.
10 Thormann M, Mpotsaris A, Behme D. Treatment of a middle cerebral artery bifurcation aneurysm with the novel Contour Neurovascular System compatible with 0.021″ catheters. *Neuroradiol J* 2022;35:396–8.
11 Biondi A, Primikiris P, Vitale G, *et al*. Endosaccular flow disruption with the Contour Neurovascular System: angiographic and clinical results in a single-center study of 60 unruptured intracranial aneurysms. *J Neurointerv Surg* 2023;15:838–43.
12 Cavasin N, Gava UA, Magrini S, *et al*. Treatment of a ruptured fetal-type posterior communicating aneurysm with a combined approach using the new Contour Neurovascular System. *BMJ Case Rep* 2022;15:e248065.
13 Dange NN, Roy JM. Initial experience with the Contour device in the treatment of ruptured intracranial wide-necked bifurcation aneurysms: a single-operator, multicenter study. *Neurol India* 2022;70:2059–64.
14 Wodarg F, Ozpeynirci Y, Hensler J, *et al*. Contour-assisted coiling with jailed microcatheter may result in better occlusion (CoCoJaMBO) in wide-necked intracranial aneurysms: proof of principle and immediate angiographic results. *Interv Neuroradiol* 2023;29:79–87.
15 Diana F, de Dios Lascuevas M, Peschillo S, *et al*. Intrasaccular flow disruptor-assisted coiling of intracranial aneurysms using the novel Contour Neurovascular Systems and NEQSTENT: a single-center safety and feasibility study. *Brain Sci* 2022;12:991.
16 Ghozy S, Lashin BI, Elfil M, *et al*. The safety and effectiveness of the Contour Neurovascular System for the treatment of wide-necked aneurysms: a systematic review and meta-analysis of early experience. *Interv Neuroradiol* 2022:15910199221139546.
17 Pravdivtseva MS, Pravdivtsev AN, Peters S, *et al*. The effect of the size of the new Contour neurovascular device for altering intraaneurysmal flow. *Interv Neuroradiol* 2023:15910199221145985.
18 Pravdivtseva MS, Peschke E, Lindner T, *et al*. 3D-printed, patient-specific intracranial aneurysm models: from clinical data to flow experiments with endovascular devices. *Med Phys* 2021;48:1469–84.
19 Pravdivtseva MS. 3D models of basilar tip intracranial aneurysms (STL) to study flow dynamics. 2021.
20 Zarrinkoob L, Ambarki K, Wåhlin A, *et al*. Blood flow distribution in cerebral arteries. *J Cereb Blood Flow Metab* 2015;35:648–54.
21 Adams R, Bischof L. Seeded region growing. *IEEE Trans Pattern Anal Machine Intell* 1994;16:641–7.
22 Lorensen WE, Cline HE. Marching cubes: a high resolution 3D surface construction algorithm. *SIGGRAPH Comput Graph* 1987;21:163–9.
23 Sindeev S, Arnold PG, Frolov S, *et al*. Phase-contrast MRI versus numerical simulation to quantify hemodynamical changes in cerebral aneurysms after flow diverter treatment. *PLoS One* 2018;13:e0190696.
24 Ouared R, Larrabide I, Brina O, *et al*. Computational fluid dynamics analysis of flow reduction induced by flow-diverting stents in intracranial aneurysms: a patient-unspecific hemodynamics change perspective. *J Neurointerv Surg* 2016;8:1288–93.
25 Pierot L, Szikora I, Barreau X, *et al*. Aneurysm treatment with the Woven EndoBridge (WEB) device in the combined population of two prospective, multicenter series: 5-year follow-up. *J Neurointerv Surg* 2023;15:552–7.
26 Pagano P, Paiusan L, Soize S, *et al*. Intracranial aneurysm treatment with intrasaccular flow disruption: comparison of WEB-21 and WEB-17 systems. *J Neurointerv Surg* 2022;14:904–9.
27 Damiano RJ, Ma D, Xiang J, *et al*. Finite element modeling of endovascular coiling and flow diversion enables hemodynamic prediction of complex treatment strategies for intracranial aneurysm. *J Biomech* 2015;48:3332–40.
28 Kulcsár Z, Augsburger L, Reymond P, *et al*. Flow diversion treatment: intra-aneurismal blood flow velocity and WSS reduction are parameters to predict aneurysm thrombosis. *Acta Neurochir* 2012;154:1827–34.
29 Briganti F, Leone G, Marseglia M, *et al*. Endovascular treatment of cerebral aneurysms using flow-diverter devices: a systematic review. *Neuroradiol J* 2015;28:365–75.
30 Goubergrits L, Schaller J, Kertzscher U, *et al*. Hemodynamic impact of cerebral aneurysm endovascular treatment devices: coils and flow diverters. *Expert Rev Med Devices* 2014;11:361–73.
31 Roloff C, Berg P. Effect of flow diverter stent malposition on intracranial aneurysm hemodynamics—an experimental framework using stereoscopic particle image velocimetry. *PLoS One* 2022;17:e0264688.
32 Kim T, Oh CW, Bang JS, *et al*. Higher oscillatory shear index is related to aneurysm recanalization after coil embolization in posterior communicating artery aneurysms. *Acta Neurochir* 2021;163:2327–37.
33 Ngoepe MN, Frangi AF, Byrne JV, *et al*. Thrombosis in cerebral aneurysms and the computational modeling thereof: a review. *Front Physiol* 2018;9:306.
34 Larrabide I, Aguilar ML, Morales HG, *et al*. Intra-aneurysmal pressure and flow changes induced by flow diverters: relation to aneurysm size and shape. *AJNR Am J Neuroradiol* 2013;34:816–22.
35 Lieber BB, Sadasivan C. Endoluminal scaffolds for vascular reconstruction and exclusion of aneurysms from the cerebral circulation. *Stroke* 2010;41:S21–5.
36 O'kelly CJ, Krings T, Fiorella D, *et al*. A novel grading scale for the angiographic assessment of intracranial aneurysms treated using flow diverting stents. *Interv Neuroradiol* 2010;16:133–7.
37 Sheng B, Wu D, Yuan J, *et al*. Hemodynamic characteristics associated with paraclinoid aneurysm recurrence in patients after embolization. *Front Neurol* 2019;10:429.
38 Pravdivtseva MS, Gaidzik F, Berg P, *et al*. Influence of spatial resolution and compressed SENSE acceleration factor on flow quantification with 4D flow MRI at 3 Tesla. *Tomography* 2022;8:457–78.
39 Bouillot P, Brina O, Delattre BMA, *et al*. Neurovascular stent artifacts in 3D-TOF and 3D-PCMRI: influence of stent design on flow measurement. *Magn Reson Med* 2019;81:560–72.

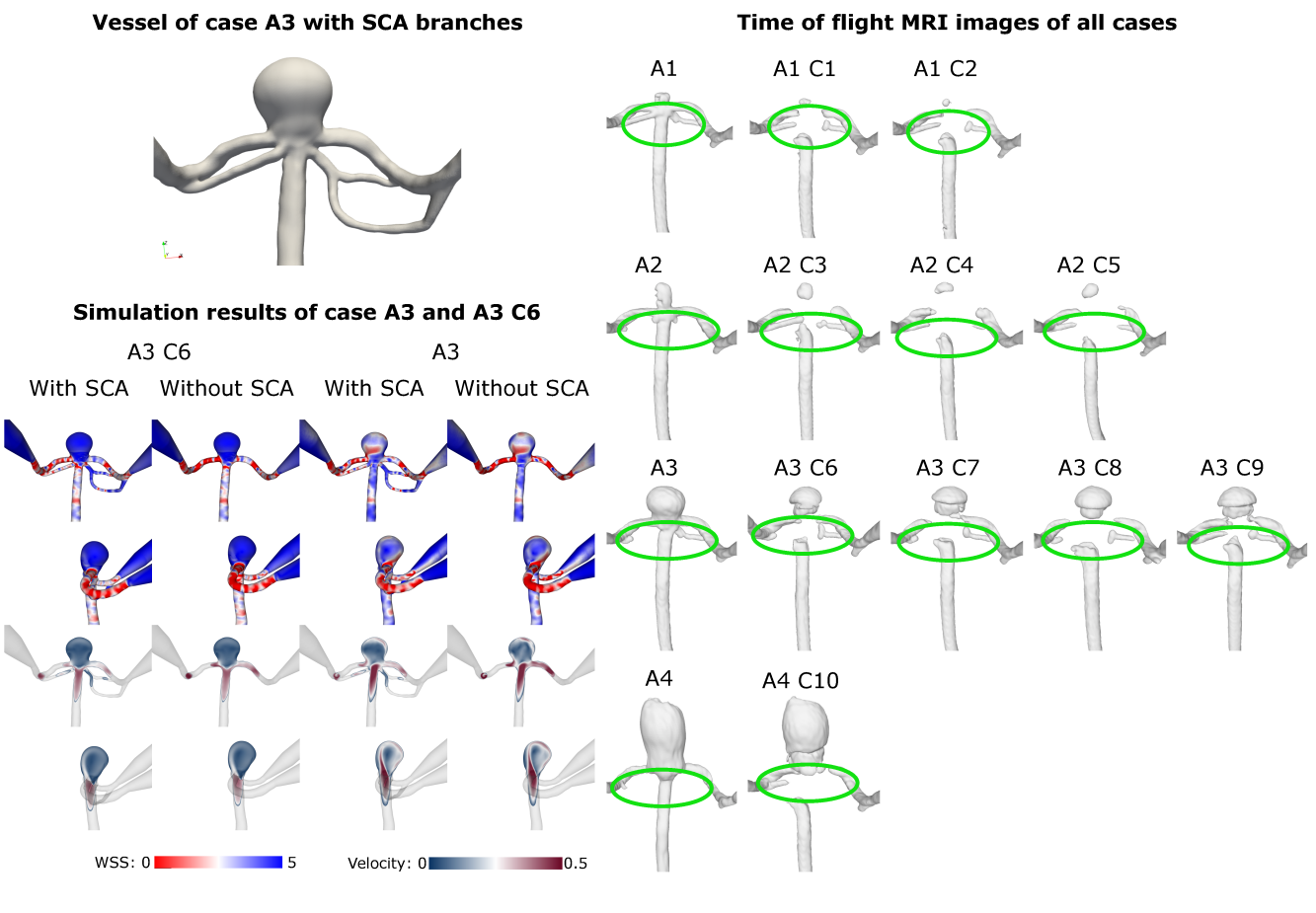

Figure S1: Top left: Vessel A2 used for 3D-printing. Bottom left: Comparison of qualitative velocity and wall shear stress patterns in A3 and A3 C6 with and without SCA vessels included. Right: Vascular segmentation from TOF MRI data of all models without (A1-A4) and with (C1-C10) Contour implanted. Notice the occluded SCA branches in most of the cases due to insufficient 3D printing (marked with green circles).

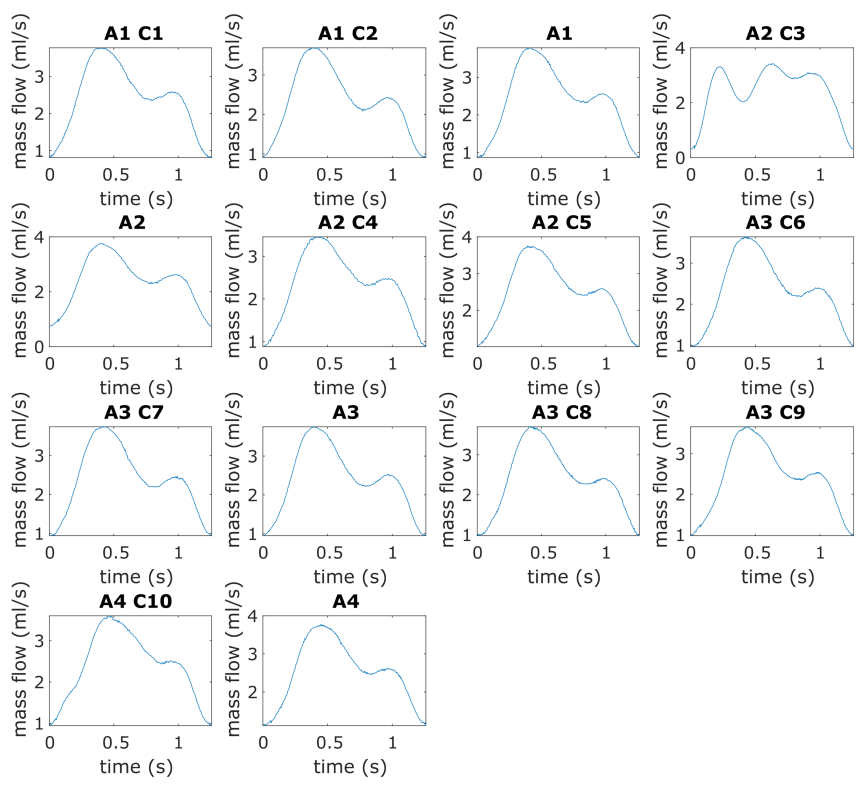

Figure S2: Mass flow curves set as boundary conditions at the inlet for each case A1-A4 and C1-C10.

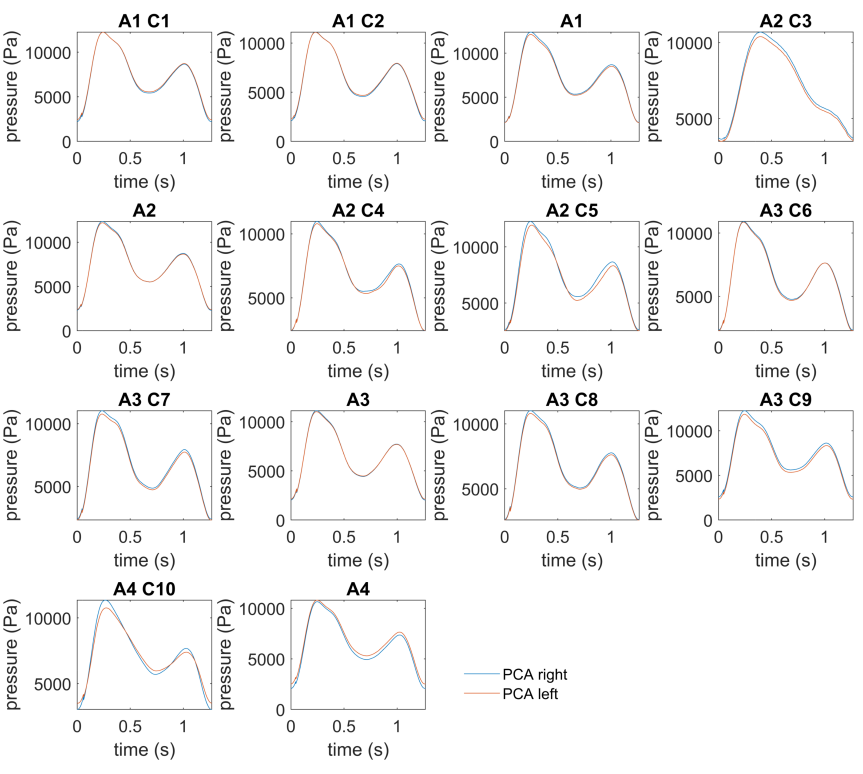

Figure S3: Pressure curves set as outlet boundary conditions for each case A1-A4 and C1-C10.

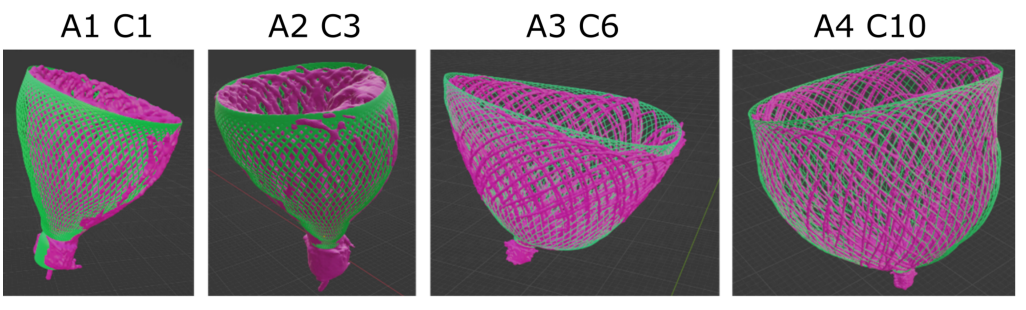

Figure S4: Visual representation of the Contour fit between virtually deformed CAD Contour (green) and µCT (pink) for four cases.

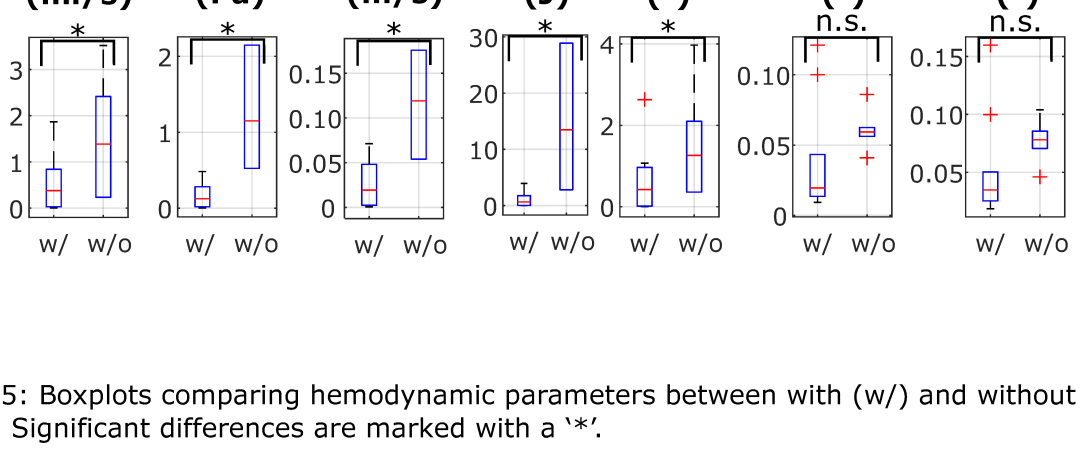

Figure S5: Boxplots comparing hemodynamic parameters between with (w/) and without (w/o) Contour. Significant differences are marked with a '*'.

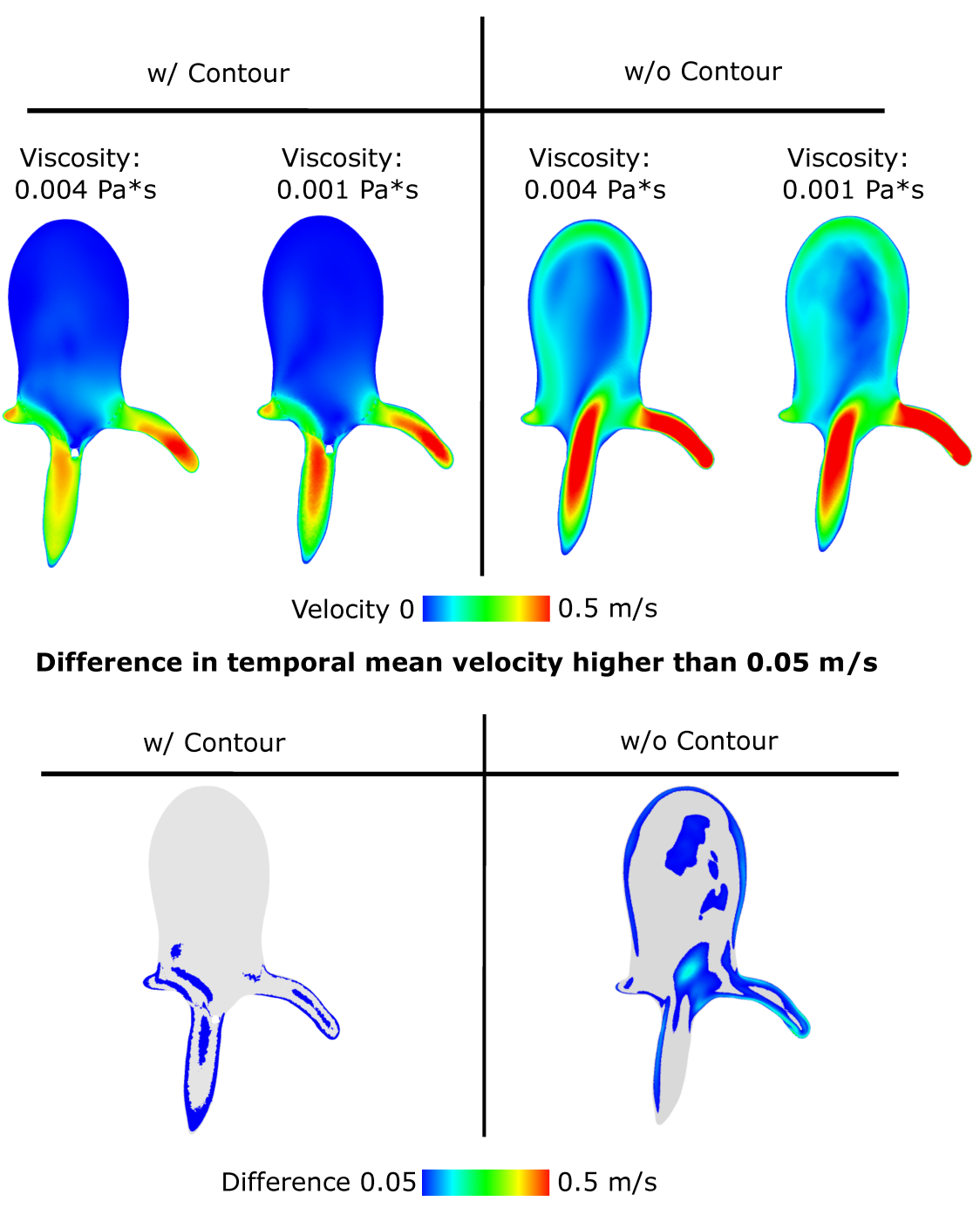

Figure S6: Comparison of the resulting velocities from CFD simulation of case A4 and A4 C10 with different viscosities (blood: 0.004 Pa*s and water: 0.001 Pa*s) and the visualization of the absolute difference in velocity higher than 0.05 m/s.

Supplementary

S1. Patient-based aneurysm models

The patient-specific vascular lumen was segmented from a clinical 3D rotational angiographic dataset (3D RA) of a patient with a basilar bifurcation tip aneurysm. To simplify the experimental setup, the distal branches were cut approximately 3 cm distally from the aneurysm neck, and the superior cerebellar arteries were combined with the posterior cerebral arteries (Fig. S1 top left). Next, the patient-specific aneurysm sac was removed and five artificial aneurysm sacs with dimensions of the aneurysm neck ranging from 2.7 to 9.7 mm were combined with the vessel lumen (Fusion 360 2.0, Autodesk, USA). The artificial aneurysms were wide-necked bifurcation aneurysms with a comparable dome-to-neck ratio (1.2±0.1). Contours sized 5, 11, and 14 mm are suitable for the resulting aneurysm based on the manufacturer's recommendations (Table S1). The models were then completed by adding an outer layer to form a vessel wall, and 3D printed (Clear Photoreactive Resin, Form 3, Formlabs, USA).

Table S1. First-generation contour neurovascular contour devices (contour): sizes and corresponding recommendations for the aneurysm sizes (Cerus Endovascular, Instructions: www.cerusendo.com/contour-neurovascular-system).

Contour Diameter (mm)	Aneurysm Neck (mm)	Aneurysm width (mm)
5	2.0 – 3.0	2.0 – 3.5
7	3.0 – 5.0	3.0 – 5.5
9	4.0 – 6.0	5.0 – 7.5
11	5.0 – 8.0	7.0 – 8.5
14	7.0 – 10.0	8.0 – 10.5

Table S2. Comparison of treatment effect (TE) without and with SCA branches for chosen hemodynamic parameters of case A3 C6.

A3 C6	TE of NIR	TE of AWSS	TE of V	TE of KE	TE of ICI	TE of OVI	TE of OSI
Without SCAs	-57%	-78%	-59%	-86%	-54%	-83%	-77%
With SCAs	-55%	-76%	-57%	-85%	-52%	-78%	-77%

Figure S1: Top left: Vessel A2 used for 3D-printing. Bottom left: Comparison of qualitative velocity and wall shear stress patterns in A3 and A3 C6 with and without SCA vessels included. Right: Vascular segmentation from TOF MRI data of all models without (A1-A4) and with (C1-C10) Contour implanted. Notice the occluded SCA branches in most of the cases due to insufficient 3D printing (marked with green circles).

S2. Flow Setup and In Vitro Device Deployment

Figure S2: Mass flow curves set as boundary conditions at the inlet for each case A1-A4 and C1-C10.

Figure S3: Pressure curves set as outlet boundary conditions for each case A1-A4 and C1-C10.

For implantation, an intermediate catheter was employed (Navien 0.072'', Medtronic, Minneapolis, MN, USA) and a microcatheter (Phenom 0.027'', Medtronic, Minneapolis, MN, USA) navigated into the center of the sac of the aneurysm model. Then, the devices were placed in the neck of the aneurysm and detached electrolytically after mechanical stability was confirmed. Angiographic contrast stasis was observed after the placement of each device indicating flow reduction at the aneurysm.

S3. Magnetic Resonance imaging

The 4D flow MRI was performed using a 3D T1-weighted spoiled fast gradient echo sequence with Cartesian sampling (echo time/repetition time: 5/8.5 msec; field of view: 110 × 110 × 40 mm^3; voxel size: (0.75 $mm)^3$; flip angle: 8°). The sequence was accelerated 4.5-fold with a compressed-sensing technique implemented by the vendor (Philips); the examination time was 41.4 minutes. For velocity encoding, a balanced symmetric 4-point phase-contrast encoding scheme (Hadamard) was used. An integrated artificial digital trigger was used for temporally resolved data acquisition, and 20 cardiac phases were obtained. The velocity-encoding parameter was set to 75 cm/s for all experiments. The velocity noise was less than 5 cm/s. The velocity noise was estimated by calculating velocity values at the static region (outside of the flow volume) in center of the imaging volume for model A4-C10.

S4. Virtual Processing Pipeline

Table S3: Quantitative comparison of geometric parameters after the deformation using the processing pipeline. RPM: Radiopaque marker. The values are averaged for the respected Contour devices (5,11,14 mm)

Geo. parameter	CN05			CN11			CN14		
	CAD	µCT	Diff [%]	CAD	µCT	Diff [%]	CAD	µCT	Diff [%]
Total length [mm]	3.63	3.7	1.89	6.49	6.99	7.21	8	8.78	8.88
Diameter average [mm]	2.5	2.53	1.19	7.15	7.16	0.14	8,56	8.76	2.28
Average grid thickness [mm]	0.02	0.07	71.43	0.02	0.08	75	0.022	0.09	75.56
Total Volume [mm^3]	9.22	10.78	14.47	135.44	140.09	3.32	325.66	330.82	1.55
Total Area [mm^2]	26.79	28.03	4.42	151.03	155	2.56	254.16	256.07	0.75

Figure S4: Visual representation of the Contour fit between virtually deformed CAD Contour (green) and µCT (pink) for four cases.

S5. Hemodynamic parameters

Oscillatory Shear Index (-): $$OSI = \frac{1}{2}\left\{1 - \frac{\frac{1}{T}\left|\int_0^T WSS\, dt\right|}{\frac{1}{T}\int_0^T |WSS| dt}\right\}$$

Oscillatory Velocity Index (-): $$OVI = \frac{1}{2} * \left\{1 - \frac{\frac{1}{T}\left|\int_0^T V\, dt\right|}{\frac{1}{T}\int_0^T |V| dt}\right\}$$

Time-averaged Wall Shear Stress (Pa): $$TAWSS = \frac{1}{T}\int_0^T |WSS| dt$$

Kinetic Energy (J): $$E_{kin} = \frac{1}{2} * \rho V^2$$

Inflow Concentration Index (-): $$ICI = \frac{Q_{inflow}/Q_{parentvessel}}{A_{inflow}/A_{ostium}}$$

Aneurysm turnover time (s): $$TOT = \frac{Volume_{IA\,sac}}{Neck\ infow\ rate}$$

S6. Results

Table S4: Detailed information about the treatment effect (%) for each case C1-10 compared to the models without Contour (A1-4) for specific hemodynamic parameters (underlying information for Figure 4a)

Contour	NIR	AWSS	V	KE	ICI	OVI	OSI
A1 C1	-0.86	-0.90	-0.88	-0.98	-0.96	-0.54	-0.60
A1 C2	-0.99	-1.00	-1.00	-1.00	-0.99	0.06	0.06
A2 C3	-0.89	-0.98	-0.96	-1.00	-0.91	-0.64	-0.29
A2 C 4	-0.84	-0.96	-0.91	-0.98	-0.96	-0.68	-0.53
A2 C 5	-0.88	-0.95	-0.96	-0.99	-0.97	1.16	1.26
A3 C6	-0.57	-0.78	-0.59	-0.86	-0.54	-0.83	-0.77
A3 C 7	-0.70	-0.87	-0.76	-0.95	-0.59	-0.78	-0.70
A3 C 8	-0.65	-0.84	-0.69	-0.93	-0.61	-0.85	-0.69
A3 C 9	-0.71	-0.87	-0.73	-0.94	-0.49	-0.65	-0.57
A4 C10	-0.47	-0.87	-1.00	-0.94	-0.34	0.16	-0.04

Figure S5: Boxplots comparing hemodynamic parameters between with (w/) and without (w/o) Contour. Significant differences are marked with a '*'

Figure S6: Comparison of the resulting velocities from CFD simulation of case A4 and A4 C10 with different viscosities (blood: 0.004 Pa*s and water: 0.001 Pa*s) and the visualization of the absolute difference in velocity higher than 0.05 m/s.